LAWRENCE
LIVERMORE
NATIONAL
LABORATORY

UCRL-JRNL-236046

Predictive wavefront control for Adaptive Optics with arbitrary control loop delays

L. A. Poyneer, J.-P. Veran

November 1, 2007

Journal of the Optical Society of America, A

Disclaimer

Predictive wavefront control for Adaptive Optics with arbitrary control loop delays

Lisa Poyneer[1,*] and Jean-Pierre Véran[2]

[1]*Lawrence Livermore National Laboratory, 7000 East Avenue, Livermore, California 94550, USA*

[2]*Herzberg Institute of Astrophysics, 5071 West Saanich Road, Victoria, British Columbia, Canada V9E2E7*

[*]*Corresponding author: poyneer1@llnl.gov*

We present a modification of the closed-loop state space model for AO control which allows delays that are a non-integer multiple of the system frame rate. We derive the new forms of the Predictive Fourier Control Kalman filters for arbitrary delays and show that they are linear combinations of the whole-frame delay terms. This structure of the controller is independent of the delay. System stability margins and residual error variance both transition gracefully between integer-frame delays.

OCIS codes: 010.1080, 010.1285,

1. Introduction

Significant research into developing advanced wavefront control techniques has recently been done in the field of Adaptive Optics (AO). Future AO systems have ambitious performance goals which will require advances beyond current wavefront control techniques. In particular, an advanced wavefront controller can help reduce the servo-lag (residual atmosphere) error which scatters light close in near the point-spread-function (PSF) core. This new research includes work by Kulcsár et al. [1] and Looze [2] in applying established control systems theory and techniques to the AO scenario. Experimental work has been done by Petit et al. [3] on using Kalman filtering for vibration reduction and by Hinnen et al. [4] in using $\mathcal{H}_2$-optimal control.

In our own recent work we have proposed a computationally feasible and adaptive predictive controller. This method is termed Predictive Fourier Control (PFC) [5] and it builds upon the closed-loop AO control with Kalman filtering framework which was developed by Le Roux et al. [6]. In PFC the wavefront is reconstructed in the Fourier basis set [7]. Under

the assumption of frozen flow atmospheric turbulence, the Fourier modes are nearly uncorrelated both spatially and temporally. This allows each complex-valued Fourier mode to be controlled independently. Closed-loop AO telemetry of the residual phase is recorded and analyzed using a temporal power spectral density (PSD) technique. This allows easy identification of atmospheric layers, which have a highly compact temporal PSD under frozen flow. State space model parameters are directly estimated from closed-loop telemetry and are then used to solve the Algebraic Riccati Equation (ARE), producing the steady-state Kalman filter which predicts the atmosphere.

The state-space model of Le Roux et al. is a discrete-time approximation to the hybrid continuous/discrete-time AO control system. This standard model (as described in [8]) is shown in Fig. 1. In this model the continuous phase aberration $\phi(t)$ is corrected in closed-loop, with discrete measurement noise $v[t]$. The wavefront sensor (WFS) integration and deformable mirror (DM) shaping are done on intervals of length T, producing a frame rate $f_{\text{ao}} = 1/T$. The total computational latency of the AO system, from the end of the WFS CCD integration to the end of the write to the deformable mirror (DM), is given by τ. If $\tau = T$, the AO system can be described with the discrete-time model of Le Roux et al. Kulcsár has shown that when τ is an integer multiple of T, and when the discrete-time phase is the average of the continuous atmospheric phase over that interval of length T, this state space model results in the optimal control algorithm [1]. If τ is a different integer multiple of T, the state space model of Le Roux can be easily modified to capture that delay.

It may not always be the case, however, that τ is an integer multiple of T. For example, in the preliminary design phase of the Gemini Planet Imager (GPI) [9], the system's WFS integration time is $T = 500$ μs and the delay is $\tau = 737$ μs. Since by its very nature a predictive controller is intimately dependent on the total system delay, it is necessary to determine what the predictive controller will be when the delay τ is a non-integer multiple of T. Furthermore, the models which we use to do Monte Carlo simulations of AO system are discrete-time, and therefore cannot simulate fractional delays.

In this paper we present a new modified state space model for the AO measurement and control for arbitrary compute delays. We address the range $0 \leq \tau \leq 2T$, though the treatment is easily extensible to longer delays, if necessary. This model allows derivation of a form of PFC for arbitrary system delays. We do not present a theoretical result (á la Kulcsár) which proves that this answer is in fact the minimum variance controller for non-integer delays. Instead, we present theory and simulation results which show the graceful behavior of variable-delay PFC between integer time step delays. The simulations are done with Simulink to specifically address the hybrid model.

2. State space model

2.A. Modeling the asynchronous DM

The discrete-time state space model mentioned above is valid when the computational delay τ is an integer multiple of T. When the delay is non-integer, however, the DM takes a new shape asynchronously with the rest of the system. We have chosen to address this by treating the discrete-time signals as if they are constant over an interval of length T, and using linear combinations of them. Looze [2] used a method termed lifting to construct a higher order state space model. We do not follow that approach but instead have pragmatically modified the existing model.

The asynchronicity and how we model it is illustrated in Fig. 2. At the top is the discrete-time version, where the WFS measurement $y[t]$ is related to the atmospheric phase $\phi[t]$ and the DM commands $d[t]$. In the $\tau = T$ case of Le Roux (which PFC uses) the measurement is delayed by one time step as $y[t] = \phi[t-1] - d[t-1]$. Using the Kalman filter result, the new DM command $d[t+1]$ is the best estimate of the phase based on the WFS measurements up to time t as $d[t+1] = \hat{\phi}[t+1|t]$.

In our new model we assume that all the signals are constant over an interval, instead of existing at discrete points. This is shown in the second row. The exact same equations hold for $\tau = T$. When the compute delay τ is less than T, the DM signals are applied earlier, which causes the DM signals to shift to the left by a fractional amount $\Delta = \tau/T - 1$, as is shown in the third row. The WFS measurement $y[t]$ still sees the phase $\phi[t-1]$, but it now observes two different shapes on the DM. It sees $d[t-1]$ for the first fraction of the interval, and $d[t]$ for the second. Written out using Δ, the measurement now is modeled as

$$y[t] = \phi[t-1] - \{-\Delta d[t] + (1+\Delta)d[t-1]\}\,. \tag{1}$$

This simply is a linear combination of the two DM signals, with the weighting dependent on the delay. The second consequence of the asynchronicity is that the new DM command $d[t+1]$ spans two phase instances. Following the approach above, the new DM command is a linear combination of the phase estimates

$$d[t+1] = -\Delta\hat{\phi}[t|t] + (1+\Delta)\hat{\phi}[t+1|t]. \tag{2}$$

When the computational delay is longer than one step, the DM signal is shifted to the right, as is shown in the fourth row of the figure. Now the measurement is

$$y[t] = \phi[t-1] - \{(1-\Delta)d[t-1] + \Delta d[t-2]\}\,, \tag{3}$$

and the DM command is

$$d[t+1] = (1-\Delta)\hat{\phi}[t+1|t] + \Delta\hat{\phi}[t+2|t]. \tag{4}$$

In this model we treat all signals as being constant over the interval, with the DM write asynchronous with the WFS read. This is the correct behavior for the DM, which is held constant. However, this is an approximation in the case of the atmospheric phase, which actually varies continuously. How much this approximation reduces the optimality of this model is left for future theoretical work.

These new measurement equations (1) and (3) will be incorporated into the state space model. The new DM command equations (2) and (4) will be used in solving the model for the predictive filter.

2.B. State space model for Fourier control

Modal Fourier reconstruction analyzes the wavefront in the complex-valued Fourier modal basis set. For a given pupil size D and subaperture size d, there are D/d subapertures across the pupil. The phase is reconstructed on an $N \times N$ grid. N is usually a few larger than D/d, and chosen for a computationally efficient discrete Fourier transform (DFT), e.g. FFTW [10]. For example, in GPI $D/d = 44$ and $N = 48$. The Fourier modes, when calculated with the DFT, are indexed by frequency variable k and l, take the values $-N/2, -(N/2-1), \cdots, -1, 0, 1, \cdots, (N/2-2), (N/2-1)$. This gives each Fourier mode the frequency components, in units of m^{-1}, $f_x = k/(Nd)$ and $f_y = l/(Nd)$.

The model of the input atmosphere is the same as in the original PFC derivation, where we assume frozen flow of layers of atmospheric phase aberration. When controlling Fourier modes, each turbulent layer becomes a first-order auto-regressive process. A complex-valued AR(1) process has the basic form

$$a[t] = \alpha a[t-1] + w[t]. \tag{5}$$

The complex number α has magnitude just less than one. The phase of α sets how much the Fourier mode advances in a single time step. This is simply $2\pi T$ times the dot product of the velocity vector of the layer with the frequency vector of that Fourier mode: $-2\pi T(kv_x + lv_y)/(Nd)$.

We assume that the atmosphere is composed of a static layer where α is a real number just less than one, and L layers of frozen flow. The state variables for these layer components are given by

$$\mathbf{a} = (a_0, a_1, \cdots, a_L) \tag{6}$$

and the auto-regression parameters are stored in the matrix

$$\mathbf{R} = \mathrm{Diag}(\alpha_0, \alpha_1, \cdots, \alpha_L). \tag{7}$$

The state space model requires the power levels of each of the driving noises, which set the amount of phase power in each layer. These are given by the covariance matrix

$$\mathbf{P}_w = \mathrm{Diag}(\sigma^2_{a_0}, \sigma^2_{a_1}, \cdots, \sigma^2_{a_L}). \tag{8}$$

In addition to the atmospheric layers, the state vector contains the phase ϕ and the DM command d at various instances in time. To capture the range of possible delays $0 \leq \tau \leq 2T$, we need 4 phase variables and 3 DM variables, making the state vector

$$\mathbf{x}[t] = (\mathbf{a}[t], \phi[t+2], \phi[t+1], \phi[t], \phi[t-1], d[t], d[t-1], d[t-2])^T. \tag{9}$$

The evolution of this state vector is governed by the equation $\mathbf{x}[t+1] = \mathbf{A}\mathbf{x}[t] + \mathbf{G}d[t+1] + \mathbf{B}\mathbf{w}[t]$. Note that the original PFC derivation used the term $\mathbf{G}d[t]$ instead of $\mathbf{G}d[t+1]$, but this is a mathematical convenience which will not affect the results. The state transition matrix is

$$\mathbf{A} = \begin{pmatrix} \mathbf{R} & \mathbf{0}_{1\times(L+1)} & \mathbf{0}_{1\times(L+1)} & \mathbf{0}_{1\times(L+1)} & \mathbf{0}_{1\times(L+1)} & \mathbf{0}_{1\times(L+1)} & \mathbf{0}_{1\times(L+1)} & \mathbf{0}_{1\times(L+1)} \\ \mathbf{1}_{(L+1)\times 1} & 0 & 0 & 0 & 0 & 0 & 0 & 0 \\ \mathbf{0}_{(L+1)\times 1} & 1 & 0 & 0 & 0 & 0 & 0 & 0 \\ \mathbf{0}_{(L+1)\times 1} & 0 & 1 & 0 & 0 & 0 & 0 & 0 \\ \mathbf{0}_{(L+1)\times 1} & 0 & 0 & 1 & 0 & 0 & 0 & 0 \\ \mathbf{0}_{(L+1)\times 1} & 0 & 0 & 0 & 0 & 0 & 0 & 0 \\ \mathbf{0}_{(L+1)\times 1} & 0 & 0 & 0 & 0 & 1 & 0 & 0 \\ \mathbf{0}_{(L+1)\times 1} & 0 & 0 & 0 & 0 & 0 & 1 & 0 \end{pmatrix}. \tag{10}$$

The matrix $\mathbf{G}$ governs the incorporation of the most recent DM command (the output of the predictive filter) into the state.

$$\mathbf{G} = (\mathbf{0}_{(L+1)\times 1}, 0, 0, 0, 0, 1, 0, 0)^T. \tag{11}$$

Finally, the driving noises are incorporated with

$$\mathbf{B} = \begin{pmatrix} \mathbf{I}_{(L+1)\times(L+1)} \\ \mathbf{0}_{(L+1)\times 7} \end{pmatrix}. \tag{12}$$

There are now two key differences from the original PFC derivation. Up to this point everything is the same as in the original model, though extra states have been added. Now the equations (1) and (3) are incorporated into the state space model measurement equation. $y[t] = \mathbf{C}\mathbf{x}[t] + v[t]$. Here $v[t]$ is the measurement noise and has variance $\mathbf{P}_v = (\sigma_v^2)$. For $\tau \leq T$ the matrix is

$$\mathbf{C}_{\tau \leq T} = (\mathbf{0}_{(L+1)\times 1}, 0, 0, 0, 1, \Delta, -(1+\Delta), 0). \tag{13}$$

In the longer delay case we have

$$\mathbf{C}_{\mathrm{T} \leq \tau} = (\mathbf{0}_{(L+1)\times 1}, 0, 0, 0, 1, 0, -(1-\Delta), -\Delta). \tag{14}$$

The second set of new equations from Section 2.A will be used in the process of solving for the predictive filter.

3. Predictive filter with arbitrary delay

Given this state space model described by the two equations $\mathbf{x}[t+1] = \mathbf{A}\mathbf{x}[t] + \mathbf{G}d[t+1] + \mathbf{B}\mathbf{w}[t]$ and $y[t] = \mathbf{C}\mathbf{x}[t] + v[t]$, we solve as originally for the temporal filter. Recall that the temporal filter is $C(\mathsf{z})$, as shown in Fig. 1.

Many AO systems use an integral controller, such as $C(\mathsf{z}) = g/(1 - 0.99\mathsf{z}^{-1})$. In the technique of modal gain optimization, which was developed by Gendron and Léna [11], the gain g is optimized. This method, done in closed-loop with Fourier modes, forms the GPI baseline control algorithm of Optimized-gain Fourier Control [7]. For PFC we will use AO telemetry to find the best $C(\mathsf{z})$, where the form of the predictor is given by the Kalman filter.

This derivation is done in two steps. First, the estimation equation, which uses the steady-state Kalman gain vector $\mathbf{K}_s$,

$$\hat{\mathbf{x}}[t|t] = (\mathbf{I} - \mathbf{K}_s\mathbf{C})\mathbf{A}\hat{\mathbf{x}}[t-1|t-1] + (\mathbf{I} - \mathbf{K}_s\mathbf{C})\mathbf{G}d[t] + \mathbf{K}_s y[t] \tag{15}$$

is solved with the Z-transform to determine the transfer function $C(\mathsf{z})$ between the measurement $y[t]$ and the new DM command $d[t+1]$. This control law will be a function of $\mathbf{K}_s$, which is in turn a function of the entries of the steady-state error covariance matrix $\mathbf{P}_s$:

$$\mathbf{K}_s = \mathbf{P}_s\mathbf{C}^{\mathrm{H}}(\mathbf{C}\mathbf{P}_s\mathbf{C}^{\mathrm{H}} + \mathbf{P}_v)^{-1}. \tag{16}$$

This matrix is found by numerically solving the Algebraic Riccati Equation (ARE):

$$\mathbf{P}_s = \mathbf{A}\mathbf{P}_s\mathbf{A}^{\mathrm{H}} + \mathbf{B}\mathbf{P}_w\mathbf{B}^{\mathrm{H}} - \mathbf{A}\mathbf{P}_s\mathbf{C}^{\mathrm{H}}(\mathbf{C}\mathbf{P}_s\mathbf{C}^{\mathrm{H}} + \mathbf{P}_v)^{-1}\mathbf{C}\mathbf{P}_s\mathbf{A}^{\mathrm{H}}. \tag{17}$$

The matrix $\mathbf{P}_s$ is indexed by column then row indices, e.g., $p_{1,0}$ is the second element in the top-most row-vector.

3.A. Solution for delays shorter than one frame

First we solve the set of equations produced by Eq. (15). For this we will use Z-tranform notation with the complex number z, and uppercase letters indicating the Z-transform of time series, e.g. $A_0(\mathsf{z})$ for $a_0[t]$. For clarity of notation we will also use dummy variables for the state vector elements. For this case we will need 3 for the phases: $l[t] = \hat{\phi}[t+2]$, $m[t] = \hat{\phi}[t+1]$ and $n[t] = \hat{\phi}[t]$.

In order to solve for the control law $C(\mathsf{z})$, we need to express its output $d[t+1]$ in terms of state variables. This is exactly what we did in (2). In Z-transform notation the predictive controller is

$$C(\mathsf{z}) = -\Delta\frac{N(\mathsf{z})}{Y(\mathsf{z})} + (1+\Delta)\frac{M(\mathsf{z})}{Y(\mathsf{z})}. \tag{18}$$

To solve this system of equations we use two helper terms, which are expressed as, dropping the z arguments for compactness,

$$S = -N\mathsf{z}^{-1}(1+\Delta[(1+\Delta)\mathsf{z}^{-1}-\Delta]) + M\mathsf{z}^{-1}(1+\Delta)[(1+\Delta)\mathsf{z}^{-1}-\Delta] + Y, \tag{19}$$

and $Q = p_{L+4,L+4} + \sigma_v^2$. The state space model produces $L+4$ equations. Each layer a_i has an equation

$$A_i\mathsf{z}^3 = A_i\alpha_i\mathsf{z}^2 + Q^{-1}Sp_{L+4,i}. \tag{20}$$

Three of the phase state variables provide the equations

$$L = \mathsf{z}^2\sum_{i=0}^{L} A_i + Q^{-1}Sp_{L+4,L+1}, \tag{21}$$

$$M = L\mathsf{z}^{-1} + Q^{-1}Sp_{L+4,L+2}, \tag{22}$$

and

$$N = M\mathsf{z}^{-1} + Q^{-1}Sp_{L+4,L+3}. \tag{23}$$

These equations can be simplified with the help of special properties of the entries of $\mathbf{P}_s$ for our model. For $m = 1, 2, 3$ and 4,

$$p_{L+4,L+m} = \sum_{i=0}^{L}\frac{p_{L+4,i}}{\alpha_i^m}. \tag{24}$$

We omit the extensive algebra necessary to solve these equations and present the resulting control law which converts the measurement $y[t]$ to the best DM command:

$$C(\mathsf{z}) = \left(Q^{-1}\sum_{i=0}^{L}\frac{p_{L+4,i}}{\alpha_i^2}\frac{1}{1-\alpha_i\mathsf{z}^{-1}}\left[(1+\Delta)-\frac{\Delta}{\alpha_i}\right]\right)\times \tag{25}$$

$$\left(1+\mathsf{z}^{-1}Q^{-1}(1+\Delta)\sum_{i=0}^{L}\frac{p_{L+4,i}}{\alpha_i^2}\left[\Delta+\frac{1-\Delta}{\alpha_i}\right]\left[\frac{1-\frac{(1+\Delta)\alpha_i-\Delta}{\Delta\alpha_i+1-\Delta}\mathsf{z}^{-1}}{1-\alpha_i\mathsf{z}^{-1}}\right]\right)^{-1}. \tag{26}$$

The final term in the equation, which is the ratio of two first-order filters, can be approximated as 1 when the angles of the α_i's are small. Given this approximation, the control law simplifies to

$$C(\mathsf{z}) = \left(Q^{-1}\sum_{i=0}^{L}\frac{p_{L+4,i}}{\alpha_i^2}\frac{1}{1-\alpha_i\mathsf{z}^{-1}}\left[(1+\Delta)-\frac{\Delta}{\alpha_i}\right]\right)\times \tag{27}$$

$$\left(1+\mathsf{z}^{-1}Q^{-1}(1+\Delta)\sum_{i=0}^{L}\frac{p_{L+4,i}}{\alpha_i^2}\left[\Delta+\frac{1-\Delta}{\alpha_i}\right]\right)^{-1}. \tag{28}$$

This assumption that the angles of the α_i's are small is a reasonable one for PFC. Given a 20 m/s wind, the highest temporal frequency seen by PFC is around 80 Hz, or just 8% of Nyquist for GPI's 2 kHz AO. This makes the angle of α 0.25 radians, which qualifies as small. This assumption does not hold in all cases. Kalman filtering, as shown by Petit et al. [3], can correct for vibration at half the Nyquist frequency. In that case the angle of α is $\pi/2$ radians. In such a case the above approximation cannot be made.

3.B. Solution for delays longer than a frame

For delays $T \leq \tau$, we use (4) to express the control law

$$C(\mathsf{z}) = (1-\Delta)\frac{M(\mathsf{z})}{Y(\mathsf{z})} + \Delta\frac{L(\mathsf{z})}{Y(\mathsf{z})}. \tag{29}$$

The equations (20) - (23) are exactly the same as before, except S now equals

$$S = -N\mathsf{z}^{-1} + [M(1-\Delta) + L\Delta]\mathsf{z}^{-2}[(1-\Delta) + \Delta\mathsf{z}^{-1}] + Y. \tag{30}$$

Again, the algebra is omitted. The end result is the control law which converts the measurement $y[t]$ to the best DM command:

$$\begin{aligned} C(\mathsf{z}) &= \left[Q^{-1}\sum_{i=0}^{L}\frac{p_{L+4,i}}{\alpha_i}\frac{1}{1-\alpha_i\mathsf{z}^{-1}}\left(\Delta + \frac{1-\Delta}{\alpha_i}\right)\right] \times & (31)\\ &\left[1 + \mathsf{z}^{-1}Q^{-1}\sum_{i=0}^{L}\frac{p_{L+4,i}}{\alpha_i^3} + \mathsf{z}^{-2}Q^{-1}\Delta(2-\Delta)\sum_{i=0}^{L}\frac{p_{L+4,i}}{\alpha_i^2}\right. & (32)\\ &\left.-\mathsf{z}^{-2}Q^{-1}\Delta(1-\Delta)\sum_{i=0}^{L}\frac{p_{L+4,i}}{\alpha_i}\frac{1-[2-\alpha_i^{-1}]\mathsf{z}^{-1}}{1-\alpha_i\mathsf{z}^{-1}}\right]^{-1}. & (33)\end{aligned}$$

As before, the final term, which is a ratio of first-order filters, can be approximated as 1 for most cases, producing

$$\begin{aligned} C(\mathsf{z}) &= \left[Q^{-1}\sum_{i=0}^{L}\frac{p_{L+4,i}}{\alpha_i}\frac{1}{1-\alpha_i\mathsf{z}^{-1}}\left(\Delta + \frac{1-\Delta}{\alpha_i}\right)\right] \times & (34)\\ &\left[1 + \mathsf{z}^{-1}Q^{-1}\sum_{i=0}^{L}\frac{p_{L+4,i}}{\alpha_i^3} + \mathsf{z}^{-2}Q^{-1}\Delta\sum_{i=0}^{L}\frac{p_{L+4,i}}{\alpha_i}\left(\frac{2-\Delta}{\alpha_i} - (1-\Delta)\right)\right]^{-1}. & (35)\end{aligned}$$

3.C. General form and implementation

These two forms of the predictive controller, (27) and (34), appear to be fairly complex algebraic expressions. However, they share the same simple underlying structure, which is illustrated in the block diagram of Fig. 3. Just as in the original PFC derivation, the predictive filter is made up of two parts: parallel first-order filters which predict each layer, and a stabilizing high-pass filter.

First the residual measurement $y[t]$ is fed through a first-order filter which we term a layer-compensating integrator. The gain on the integral controller is given by K_i. From (27) and (34) this gain is

$$K_i = \begin{cases} Q^{-1}p_{L+4,i}\alpha_i^{-2}\left[(1+\Delta) - \Delta\alpha_i^{-1}\right] & \text{if } -1 \leq \Delta \leq 0, \\ Q^{-1}p_{L+4,i}\alpha_i^{-1}\left[\Delta + (1-\Delta)\alpha_i^{-1}\right] & \text{if } 0 \leq \Delta \leq 1. \end{cases} \tag{36}$$

This gain predicts the WFS measurement by the proper amount for that specific layer, and provides a scaling based on relative strengths of the layers.

The high-pass filter (which is a lead filter) is usually either first or second order. The two coefficients D_1 and D_2 are given by

$$D_1 = \begin{cases} Q^{-1}(1+\Delta)\sum_{i=0}^{L} p_{L+4,i}\alpha_i^{-2}\left[\Delta + (1-\Delta)\alpha_i^{-1}\right] & \text{if } -1 \leq \Delta \leq 0, \\ Q^{-1}\sum_{i=0}^{L} p_{L+4,i}\alpha_i^{-3} & \text{if } 0 \leq \Delta \leq 1, \end{cases} \tag{37}$$

and

$$D_2 = \begin{cases} 0 & \text{if } -1 \leq \Delta \leq 0, \\ Q^{-1}\Delta\sum_{i=0}^{L} p_{L+4,i}\alpha_i^{-1}\left[(2-\Delta)\alpha_i^{-1} - (1-\Delta)\right] & \text{if } 0 \leq \Delta \leq 1. \end{cases} \tag{38}$$

This consistency in structure makes the predictor easy to implement in a system with variable computational delays. The structure is the same while the exact filter coefficients change with delay. Each filter coefficient K_i, D_1 or D_2 can depend on both Δ and the entries of the steady-state error covariance matrix $\mathbf{P}_s$.

However, $\mathbf{P}_s$ does not depend on Δ. This is clear based on an examination of the ARE (17). The DM commands in the state vector are known, because the matrix $\mathbf{G}$ incorporates $d[t]$ into the state vector, where it is passed along. This means that the last three rows and columns of $\mathbf{P}_s$ must be zero, since the variance of a known quantity is zero. When either $\mathbf{C}_{\tau \leq T}$ or $\mathbf{C}_{T \leq \tau}$ is used in the ARE, all the entries which contain Δ are multiplied by zeroes in $\mathbf{P}_s$. Hence the value of Δ does not affect $\mathbf{P}_s$. This means that the ARE can be solved independently from knowledge of the exact delay τ.

Particular filter forms and the implications of these conclusions will be discussed further in the specific example of a single layer.

3.D. Exploring the predictor for one layer

Let's look at the controller for the case of one layer for five different possible values or ranges of τ. For this case we assume that the atmosphere is composed of a single layer of frozen flow and that no static errors exist. The complex-valued parameter α encodes the phase change with one time step. Multiplication by α is equivalent to predicting by one time step. In the case of a single layer, the coefficients of the predictive filter can be parameterized by a real-valued gain g which ranges from 0 to 1,

$$g = \frac{p_{L+4,L+4}}{p_{L+4,L+4} + \sigma_v^2} = Q^{-1} p_{L+4,L+4}. \tag{39}$$

This gain g is a function of the SNR.

Given g, we can simplify the equations for the filter coefficients. We focus on (36), which

is the gain of the layer integrator,

$$K = \begin{cases} g\alpha & \text{if } \Delta = -1, \\ -\Delta g\alpha + (1+\Delta)g\alpha^2 & \text{if } -1 \le \Delta \le 0, \\ g\alpha^2 & \text{if } \Delta = 0, \\ (1-\Delta)g\alpha^2 + \Delta g\alpha^3 & \text{if } 0 \le \Delta \le 1, \\ g\alpha^3 & \text{if } \Delta = 1. \end{cases} \tag{40}$$

In the case of integer delays, the coefficient K is a gain (based on the SNR) and a prediction by the appropriate number of time steps. For example, if the $\tau = T$ case there is a delay of 2 whole steps between the WFS integration interval and the interval where the new DM commands are applied. Multiplication by α^2 predicts by two steps. When the delay is a non-integer multiple of T, the coefficient K does a linear approximation with the nearest whole delays. This linear approximation is a good one, particularly when the angle of α is small, which we assume it is.

So the layer-integrator coefficient K has two functions - it scales the residual input by a gain g based on the SNR, then it predicts the measurement by the correct fractional number of steps between WFS and DM. The previous DM command is always predicted by one time step, as would be expected.

In our model for arbitrary delays (see Fig. 2) we assumed that the WFS measurements and best DM commands involved a linear combination of the overlapping intervals. The end result is a predictor which deals with non-integer delays by doing the same linear interpolation of the control for whole-integer delays.

4. Controller modeling and analysis

In this study we use two complementary methods to analyze the qualities and performance of the predictor controller. Both of these methods begin with the hybrid continuous/discrete-time model of Fig. 1.

4.A. Laplace transform equations

As is explained by Madec [8], the hybrid system can be modeled with the Laplace transform for the continuous elements, and a mapping of discrete z to continuous s for the control law. The WFS integrates over one interval from t to $t+T$. This can be represented as the difference of the integral from 0 to $t+T$ and the integral from 0 to t, which in Laplace notation is $W(\mathsf{s}) = [1 - \exp(-\mathsf{s}T)]/(\mathsf{s}T)$. The DM is a zero-order hold, where a shape is placed on the mirror and help for one time step. This zero-order hold is not linear-time-invariant, and as such is approximately modeled with the same transfer function as the WFS, $D(\mathsf{s}) = [1 - \exp(-\mathsf{s}T)]/(\mathsf{s}T)$. The DM transfer function which describes its temporal behavior is assumed to be 1, since most DMs have first resonances well above our frame rate.

The computational delay is simply $\exp(-\mathsf{s}\tau)$. To include both the continuous and discrete transfer functions, the substitution $\mathsf{z} = \exp(\mathsf{s}T)$ is made. Using this method, analytic transfer functions which describe system performance are easily determined. The error transfer function, which describes the system response from atmospheric input $\phi(t)$ to residual error $\varepsilon(t)$ is

$$H_e(f) = \frac{1}{1 + W(\mathsf{s})C(\mathsf{z} = \exp(\mathsf{s}T))\exp(-\mathsf{s}\tau)D(\mathsf{s})}. \tag{41}$$

The noise transfer function from WFS noise $v[t]$ to $\varepsilon(t)$ is

$$H_n(f) = \frac{-C(\mathsf{z} = \exp(\mathsf{s}T))\exp(-\mathsf{s}\tau)D(\mathsf{s})}{1 + W(\mathsf{s})C(\mathsf{z} = \exp(\mathsf{s}T))\exp(-\mathsf{s}\tau)D(\mathsf{s})}. \tag{42}$$

These transfer functions can be used to find the margins of the system or to estimate performance given known PSDs for the atmosphere and noise.

4.B. Simulink model

The elements of the AO control loop are implemented in Simulink. The Simulink model is shown in Fig. 4. Our model is similar to that in [2]. Because Simulink blocks vary in their ability to handle complex numbers, junctions are used to switch back and forth from a single complex-valued signal and two real-valued signals (real and imaginary parts) as appropriate. The WFS block is implemented exactly as given by the function $W(\mathsf{s})$ above. The servo lag of the system $\exp(-\mathsf{s}\tau)$ is moved up (with no loss of model accuracy) into the WFS module to ensure correct continuous-time implementation of the delay. The WFS module gain block handles the sampling conversion from continuous to discrete, after which the WFS noise is added. The residual as measured by the WFS is fed through either the integral controller or the PFC Kalman filter. The switch port provides the choice of which controller to use. The DM is implemented with a Simulink zero-order hold block, as opposed to the approximate Laplace model given above.

The simulation begins with the phase aberration input at `datainReal` and `datainImag`. This input signal is generated following the model used for the Kalman filter; see (5) - (8). This input is sampled at 100 times f_{ao} to minimize the necessary interpolation. The Simulink model saves two signals at 10 times f_{ao}: the input phase as `simin` and the residual error as `simout`. Oversampling from the frame rate is necessary to prevent aliasing errors in signal analysis. The baseline AO run is 16384 AO steps, or roughly 8 seconds.

These output signals are analyzed to produce estimates of the temporal PSDs and of the transfer functions of the system. The performance metric is the total power (variance) of the residual error $\varepsilon(t)$. This can be computed directly in the time domain from the variance of `simout`, or in the frequency domain through integration of the PSD estimate. This PSD estimate is done with the averaged, modified periodogram technique [12].

The transfer functions of the system can also be determined from the simulation outputs. To measure $|H_e(f)|^2$, the input signal $\phi(t)$ is band-limited white noise and the WFS noise level is set to zero. Then `simin` is used to estimate the input PSD $\hat{P}_\phi(f)$ and `simout` is used to estimate the residual error PSD $\hat{P}_\varepsilon(f)$. The error transfer function is then

$$|\hat{H_e(f)}|^2 = \frac{\hat{P}_\varepsilon(f)}{\hat{P}_\phi(f)}. \tag{43}$$

Likewise this can be done for the noise transfer function by having zero atmospheric input and white noise on the WFS.

4.C. Comparing the two techniques

The error transfer functions for an $L = 3$ predictive controller with $\tau = 1.5T$, as determined by theory and by Simulink, are shown in Fig. 5. The noise transfer functions are shown in Fig. 6. The theoretical form and the Simulink form do have slight differences, particularly at higher temporal frequencies. This is to be expected, because the DM transfer function used in the Laplace method is only an approximation to the actual behavior of the zero-order hold block in Simulink. When integrated over the frequency domain from $f = -f_{\mathrm{ao}}/2$ to $f = f_{\mathrm{ao}}/2$, the actual discrepancy is quite small - the integral of the Laplace transfer function is within $< 1\%$ of the Simulink result.

The result that there is little difference between the Laplace model and the Simulink model does not agree with the recent conclusion of Looze [2]. This could be due to the fact that we consistently use the variable substitution $\mathsf{z} = \exp(\mathsf{s}T)$ for all z terms in the controllers, whereas Looze uses a mix of this transform and the bilinear transform.

4.D. Stability

Though the AO control system is modeled in Simulink, the transport delay in the WFS poses significant problems when it comes to linearizing and discretizing the model for analysis of margins in Matlab. Given this, and the good agreement of the Laplace transfer functions with the Simulink model, we instead evaluate the stability margins directly by numerical analysis of the Laplace transfer functions.

Just as with the original PFC, the control law $C(\mathsf{z})$ itself is assured to be stable by the model structure of the Kalman filter. As long as the magnitudes of the α_i's are all less than one, the Kalman filter is stable. To analyze the gain and phase margins, we examine $W(\mathsf{s})C(\mathsf{z} = \exp(\mathsf{s}T))\exp(-\mathsf{s}\tau)D(\mathsf{s})$ using standard techniques [13]. The baseline stability requirements are that the phase margin is at least 45 degrees and the gain margin is at least 2. For the controllers with which we deal here, if one of these requirements is met, the other is as well.

Fig. 7 gives the phase margins for the case of a high SNR, where the controllers will be most aggressive in pushing the system margins. In fact, for most delays the optimal-gain controller is limited to the maximum gain which produces a phase margin of 45 degrees. The predictor, however, has larger margins. For the non-integer step delays, the phase margins follow a near linear interpolation between $\tau = 0$, $\tau = T$ and $\tau = 2T$. This example illustrates one advantage of the predictor over the integral controller: at high SNRs the predictor does not run into the same limitation on gain set by stability, which allows it to provide much better correction. This will be covered in more detail below. For lower SNRs the phase margins are larger for both controllers.

5. Results

5.A. Methods and cases examined

For performance analysis we have picked a specific case which is reasonable given GPI parameters. In this case $L = 3$. For $i = 0$ to L, $|\alpha_i| = 0.99$. The layer temporal frequencies are -40, 13 and 63 Hz. (As noted above, given a 20 m/s wind, a GPI Fourier mode will see layer frequencies up to 80 Hz). The distribution of driving white noise power is $\sigma^2_{a_0} = 3$, $\sigma^2_{a_1} = 2$, $\sigma^2_{a_2} = 0.5$ and $\sigma^2_{a_3} = 1$. Given this distribution, the total power in $\phi[t]$ is normalized to be 1. Then the noise power level is set by fixing the SNR, which is defined as the ratio of the standard deviations σ_ϕ/σ_v. The frame rate is $f_{\text{ao}} = 2000$ Hz, which makes $T = 500$ μs. The controller delay τ can be varied from 125 μs to 2000 μs, in increments of 125 μs, or $T/4$.

The predictive controller was determined by using the above model parameters and numerically solving the ARE (as described in detail in [5]). For comparison to the predictor, an integral controller was used and its gain was optimized, as is the baseline GPI strategy of Optimized-gain Fourier Control (OFC) [7]. In the OFC proposal, the power on the measurements (given by $y[t]$ in Fig. 1) is minimized, and a Z-transform description of the system is used. For this new arbitrary control loop delay formulation, the Laplace transfer functions will be used. A second discrepancy from the proposal is that the assumption that allowed the measurements $y[t]$ to be minimized as a proxy to the residual error $\varepsilon(t)$ [14] appears to be no longer valid. This assumption was based on the fact that the new WFS noise seen by the measurements is uncorrelated with the residual error. This can also be viewed as the assumption that $\int P_y(f) - P_\varepsilon(f)\, df$ is not a function of g. In the fractional delay case this does not hold for our model. This has implications for actual implementation of OFC with arbitrary delays, as it may require that the signal and noise PSDs be separated out of the joint estimate.

Given this, we directly minimize the residual error through the known power spectra of the input and noise and the transfer functions. This minimization of $P_\phi(f)|H_e(f)|^2 + P_v(f)|H_n(f)|^2$, where the transfer functions were given in (41) and (42), produces the gain

g. For any given τ, a maximum gain limit is determined such that the phase margin is 45 degrees at this gain. For example, when $\tau = 1.5T$, the maximum gain is 0.406. Because we find little discrepancy between the Laplace model and the Simulink model, the gains as optimized by Laplace produce the best performance in Simulink.

5.B. Performance

The simulations to study performance of the predictor with variable delays was conducted in Simulink, as described above. The performance metric is the power (variance) of the residual error. This quantity was calculated over the 8 seconds of operation for a variety of SNRs and delays. The residual error powers for low and high SNRs are shown in Fig. 8. The Simulink results are given by dots; the theoretical predictions based on the Laplace model are given with lines. There is very good agreement between the two, which should be expected since there are only small differences between the models. The predictor behaves in a graceful fashion for non-integer delays: the residual error essentially follows a linear interpolation of the performance at whole time steps.

A second important result is that the predictor improves its advantage over the integrator as delays increase. At SNR = 10, the predictor has 20% less residual error at the shortest delay and 55% less error at the longest delay. The predictor here has the same performance at $\tau = 2T$ as the optimized integrator at $\tau = T$, which mean that for this specific input the predictor enables an extra delay of 500 μs. At SNR = 1, the predictor starts out with 30% less error, which is increased to 40% less error at the longest delay. At SNR = 1 the predictor at all delays had less error than the integral controller at the shortest delay for this input atmosphere.

Some of this advantage comes from the fact that as the delay increases, the predictor has an adjustable lead filter, the coefficients of which are given in (37) and (38). As the delay increases, a lead filter appears and then becomes higher order, providing the best adjustment for each delay. In contrast, the integral controller form is fixed for all delays.

The other part of this advantage is due to the fact that the predictor can selectively correct specific temporal frequencies. Each layer which is in the model results in a notch in the error transfer function, leading to improved rejection of that component. The depth of the notch is partly a function of the power in the layer. In this manner, the predictor can selectively attenuate the input, while still limiting noise amplification. In contrast, the gain-optimized integrator must adjust its rejection simultaneously at all temporal frequencies.

6. Conclusion

We have modified the discrete-time state-space model of a hybrid continuous/discrete-time AO control system to deal with arbitrary control loop delays. This modification is used to

generate a new general formula for Predictive Fourier Control. The fundamental structure of the predictive control law is independent of the exact system delay, resulting is ease of implementation. Furthermore, the fundamental coefficients (such as the SNR-based gain for each layer) are independent of the delay. Only the amount of prediction and the specific structure of the stabilizing lead filter depend on the the delay τ.

The new PFC controller is essentially a linear interpolation of the controllers at integer-time step delays. Consequently, system stability and performance transition gracefully between these whole-step delays. Performance analysis with a complete Simulink model of the hybrid system has confirmed the efficacy of the Laplace transform model, as well as providing performance results. As the computational delay τ increases, PFC provides more of an advantage over a gain-optimized integral controller. This is because it can selectively correct specific temporal frequency bands and does not have the same strong limitations due to stability.

Acknowledgments

The authors would like to thank Bruce Macintosh for his insightful commentary during our research for this paper. This work performed under the auspices of the U.S. Department of Energy by Lawrence Livermore National Laboratory in part under Contract W-7405-Eng-48 and in part under Contract DE-AC52-07NA27344. The document number is UCRL-JRNL-236046. This work has been supported by the National Science Foundation Science and Technology Center for Adaptive Optics, managed by the University of California at Santa Cruz under cooperative agreement No. AST - 9876783.

References

1. C. Kulcsár, H.-F. Raynaud, C. Petit, J.-M. Conan, and P. V. de Lesegno, "Optimal control, observers and integrators in adaptive optics," Opt. Exp. **14**, 7464–7476 (2006).
2. D. Looze, "Discrete-time model of an adaptive optics systems," J. Opt. Soc. Am. A **24**, 2850–2863 (2007).
3. C. Petit, J.-M. Conan, C. Kulcsar, H.-F. Raynaud, T. Fusco, J. Montri, and D. Rabaud, "First laboratory demonstration of closed-loop kalman based optimal control for vibration filtering and simplified MCAO," Proc. SPIE **6272**, 62721T (2006).
4. K. Hinnen, M. Verhagen, and N. Doelman, "Exploiting the spatiotemporal correlation in adaptive optics using data-driven $\mathcal{H}_2$-optimal control," J. Opt. Soc. Am. A **24**, 1714–1725 (2007).
5. L. A. Poyneer, B. A. Macintosh, and J.-P. Véran, "Fourier transform wavefront control with adaptive prediction of the atmosphere," J. Opt. Soc. Am. A **24**, 2645–2660 (2007).

6. B. Le Roux, J.-M. Conan, C. Kulcsar, H.-F. Raynaud, L. M. Mugnier, and T. Fusco, "Optimal control law for classical and multiconjugate adaptive optics," J. Opt. Soc. Am. A **21**, 1261–1276 (2004).
7. L. A. Poyneer and J.-P. Véran, "Optimal modal Fourier transform wave-front control," J. Opt. Soc. Am. A **22**, 1515–1526 (2005).
8. P.-Y. Madec, "Control techniques," in *Adaptive Optics in Astronomy,* , F. Roddier, ed. (Cambridge University Press, 1999), pp. 131–154.
9. B. A. Macintosh, "Gemini planet imager preliminary design document volume 2: Instrument design," Tech. rep., Lawrence Livermore National Lab submitted to International Gemini Project Office (2007).
10. M. Frigo and S. G. Johnson, "The design and implementation of FFTW3," Proceedings of the IEEE **93**, 216–231 (2005).
11. E. Gendron and P. Léna, "Astronomical adaptive optics I. Modal control optimization," Astron. Astrophys. **291**, 337–347 (1994).
12. A. V. Oppenheim, R. W. Schafer, and J. R. Buck, *Discrete-time Signal Processing* (Prentice Hall, New Jersey, 1999).
13. A. V. Oppenheim, A. S. Willsky, and S. H. Nawab, *Signals and Systems (2nd Ed.)* (Prentice Hall, New Jersey, 1997).
14. C. Dessenne, P.-Y. Madec, and G. Rousset, "Optimization of a predictive controller for closed-loop adaptive optics," Appl. Opt. **37**, 4623–4633 (1998).

List of Figure Captions

Fig. 1 Block diagram of hybrid continuous/discrete-time AO control loop for a single Fourier mode. The phase aberration $\phi(t)$ is corrected in closed-loop in the presence of measurement noise $v[t]$. The WFS dynamics are represented by $W(\mathsf{s})$, the DM dynamics by $D(\mathsf{s})$ and the controller delay by $\exp(-\mathsf{s}\tau)$. The discrete-time control law is $C(\mathsf{z})$.

Fig. 2 Comparison of discrete-time state space model for delay $\tau = T$ (row 1) to the new model, which assumes the signals are constant over an the interval of the sampling period (row 2). When $\tau \leq T$, the DM signal shifts to the left and becomes asynchronous (row 3). When $T \leq \tau$, the DM signal shifts to the right (row 4).

Fig. 3 Flow diagram illustrating implementation of predictive filter for $0 \leq \tau \leq 2T$. The coefficients used in the filter depend on Δ, and are taken from Eq (27) or Eq (34). Note that when $\tau \leq T$, $D_2 = 0$.

Fig. 4 Simulink model of the hybrid continuous/discrete-time AO control loop for a complex-valued Fourier modal coefficient. The WFS module implements the standard transfer function $W(\mathsf{s})$, while the DM module is a Simulink zero-order hold block. The integral controller and Kalman filters are implemented with discrete-time blocks of gains and delays. (The Kalman block is implemented exactly as in Fig. 3). A switch allows use of either controller.

Fig. 5 Error transfer function for a predictive controller with $\tau = 1.5T$, based on Laplace transform model or as determined by running white noise through Simulink model. There are some small discrepancies, due to the modeling of the DM.

Fig. 6 Noise transfer function for a predictive controller with $\tau = 1.5T$, based on Laplace transform model or as determined by running white noise through Simulink model. There are some small discrepancies, due to the modeling of the DM.

Fig. 7 Phase margins for a high-SNR case for the optimized gain integrator and the predictor. For most delays τ the optimal gain is limited to be the maximum gain set by stability. The predictor can be more aggressive and has larger margins for all τ.

Fig. 8 Residual error from Simulink simulation, for predictor and optimized-gain integrator, for SNRs of 1 and 10. Simulink results are given with data points, Laplace model results are given as lines.

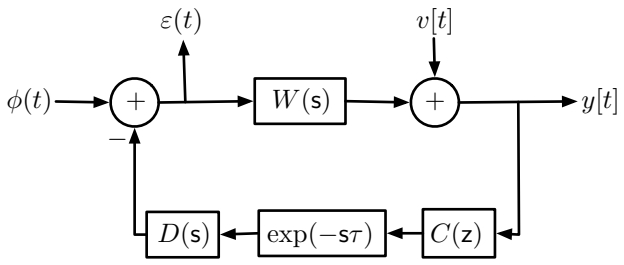
$\varepsilon(t)$
$v[t]$
$\phi(t)$
+
−
$W(\mathsf{s})$
+
$y[t]$
$D(\mathsf{s})$
$\exp(-\mathsf{s}\tau)$
$C(\mathsf{z})$

Fig. 1.

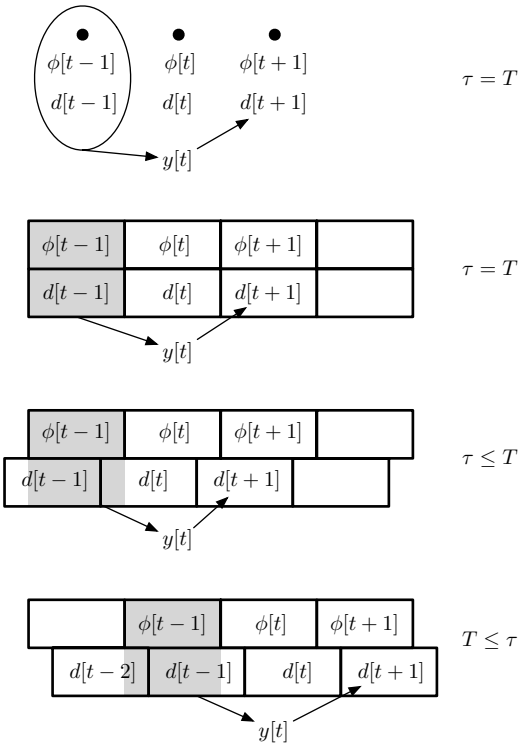
$\phi[t-1]$
$d[t-1]$
$\phi[t]$
$d[t]$
$\phi[t+1]$
$d[t+1]$
$y[t]$
$\tau = T$
$\phi[t-1]$
$\phi[t]$
$\phi[t+1]$
$d[t-1]$
$d[t]$
$d[t+1]$
$y[t]$
$\tau = T$
$\phi[t-1]$
$\phi[t]$
$\phi[t+1]$
$d[t-1]$
$d[t]$
$d[t+1]$
$y[t]$
$\tau \leq T$
$\phi[t-1]$
$\phi[t]$
$\phi[t+1]$
$d[t-2]$
$d[t-1]$
$d[t]$
$d[t+1]$
$y[t]$
$T \leq \tau$

Fig. 2.

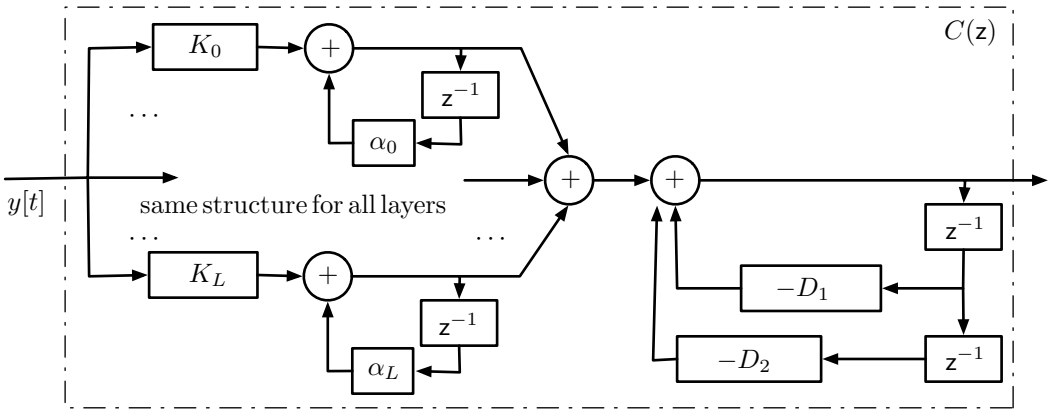

Fig. 3. [Do not reduce]

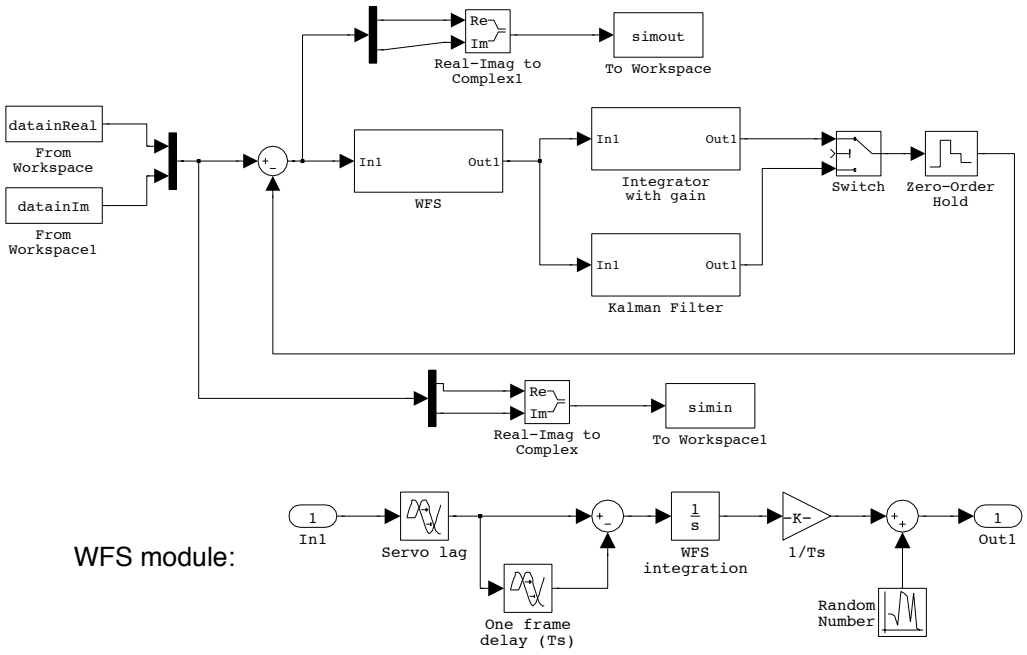

Fig. 4. [Do not reduce]

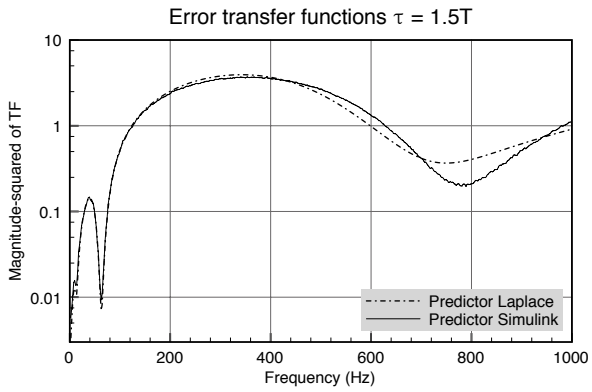
Error transfer functions τ = 1.5T
Magnitude-squared of TF
Frequency (Hz)
10
1
0.1
0.01
0
200
400
600
800
1000
Predictor Laplace
Predictor Simulink

Fig. 5.

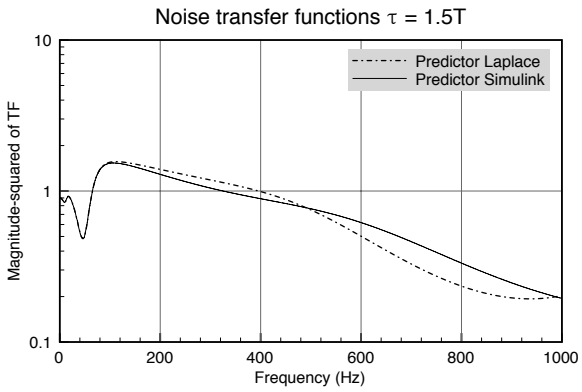
Noise transfer functions τ = 1.5T
Predictor Laplace
Predictor Simulink
Magnitude-squared of TF
Frequency (Hz)
10
1
0.1
0
200
400
600
800
1000

Fig. 6.

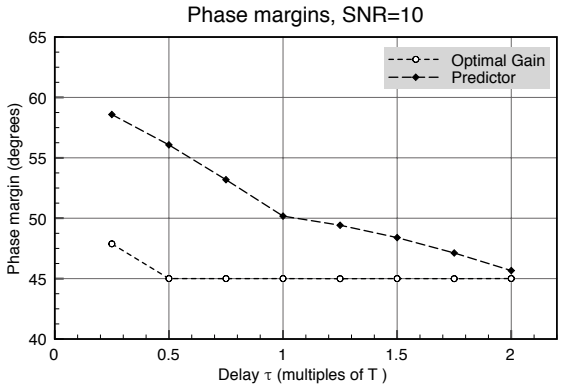
Phase margins, SNR=10
Optimal Gain
Predictor
Phase margin (degrees)
Delay τ (multiples of T)
65
60
55
50
45
40
0
0.5
1
1.5
2

Fig. 7.

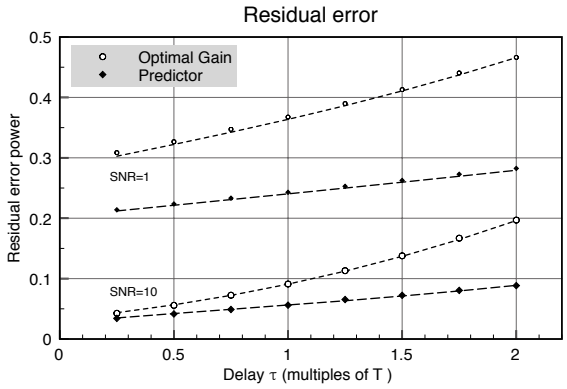
Residual error
Optimal Gain
Predictor
SNR=1
SNR=10
Residual error power
Delay τ (multiples of T)
0
0.1
0.2
0.3
0.4
0.5
0
0.5
1
1.5
2

Fig. 8.